
THE ISCHEMIC PENUMBRA

Edited by

Geoffrey A. Bonman

Jean-Cluude Baron

Stephen M. Davis

Frank R. Sharp

1
2
3
4
5
6
7
8
9
10
11
12
13
14
15
16
17
18
19
20
21
22
23
24
25
26
27
28
29
30
31
32
33
34
35
36
37
38
39
40
41
42
43
44
45
46
47
48
49
50
51
52
53
54
55
56

13 Magnetic Resonance Imaging Assessment of the Ischemic Penumbra in Experimental Stroke

move down

Timothy Q. Duong

Yerkes Imaging Center, Division of Neuroscience and Department of Neurology, Emory University, Atlanta, Georgia, U.S.A.

Marc Fisher

UMASS/Memorial Healthcare, Worcester, Massachusetts, U.S.A.

University of Massachusetts

QUANTITATIVE PERFUSION AND DIFFUSION IMAGING

Diffusion-weighted magnetic resonance imaging (MRI) has become an established method for noninvasive evaluation of cerebral ischemia in both humans and animal models. Although the biophysical mechanism(s) underlying apparent diffusion coefficient (ADC) reduction in ischemic tissue remains poorly understood (1–4), diffusion-weighted imaging (DWI) (1) is widely recognized for its ability to noninvasively detect ischemic brain injury within minutes after its onset, whereas other conventional imaging techniques [such as T₁-, T₂-weighted MRI, Computed Tomography (CT)] fail to detect such injury for at least several hours (1). Brain tissues with perfusion deficits below a critical threshold level [e.g., a cerebral blood flow (CBF) value of ~20 mL/100 g/min in rat or gerbil brain] (5,6) experience metabolic energy failure, membrane depolarization, and subsequent cellular swelling (cytotoxic edema). These changes precipitate a reduction in the ADC of brain water that is manifested as a hyperintense region on a DWI (1). Perfusion-weighted imaging (PWI) evaluates blood flow in the microcirculation of the brain and can be performed with either a bolus contrast technique or an arterial spin labeling technique (7,8). The latter approach provides relatively higher sensitivity and allows repeated measures for increased spatial resolution, but is less widely used because it is relatively more difficult to perform. During the first few hours after stroke onset (i.e., the acute phase), the anatomic region encompassed by the DWI abnormality is typically smaller than the volume of the perfusion deficit, but it usually expands and eventually coincides with the PWI volume (6,9). The difference in the regions of the PWI and DWI abnormality during the acute phase of stroke has been termed the “perfusion–diffusion” mismatch (PWI/DWI mismatch), and it was suggested that this region of mismatch approximates potentially salvageable ischemic tissue or the ischemic penumbra (10).

In humans, a “perfusion–diffusion mismatch” has been widely observed and it persists for many hours after stroke onset (10). Although the precise imaging identification of the ischemic penumbra requires correlation with regions of disturbed energy metabolism [as rigorously investigated on animal models (11–13)], such correlation is generally not possible in humans. Therefore, identification of the ischemic penumbra and viability thresholds have been operationally defined based on DWI, PWI, and other equivalent imaging modalities (14–16). The transition from potentially reversible to irreversible ischemic injury is a complex process that is highly dependent on the duration and severity of ischemia, and as such different subsets of the ischemic penumbra could have variable outcomes. Re-establishing tissue perfusion and/or administering neuroprotective drugs in a timely fashion could be expected to salvage some portions of the ischemic penumbra (17,18). For example, clinical trials have demonstrated the benefits of thrombolytic therapy using recombinant tissue plasminogen activator (t-PA) within three hours after the onset of ischemia and the clinical benefit was associated with smaller late infarcts on CT (18). It is therefore plausible to presume that early intravenous t-PA use likely salvages a portion of the ischemic penumbra, and preliminary studies support this hypothesis. To potentially help to

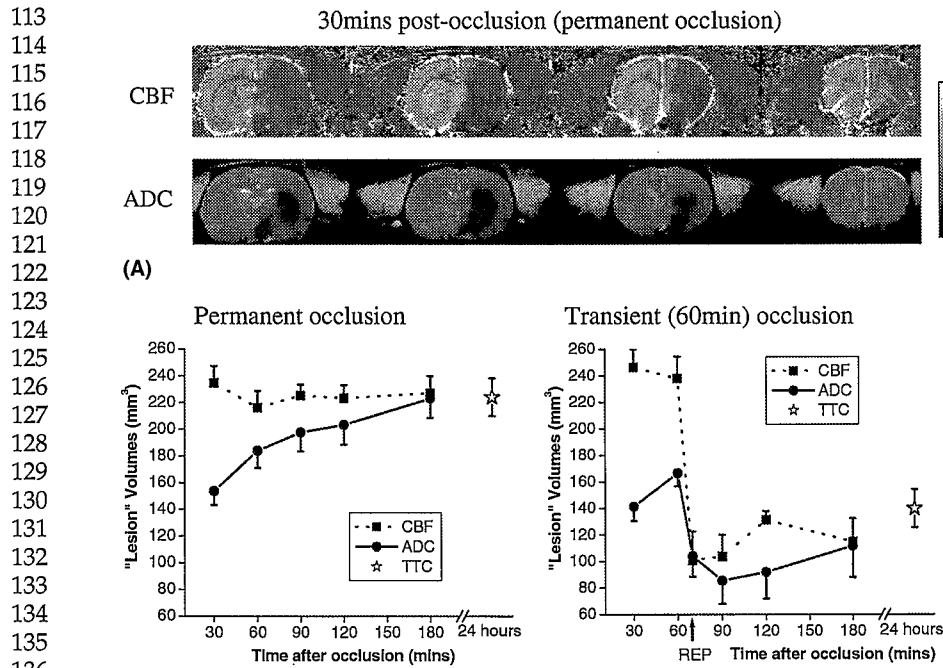
57 expand the time window for thrombolytic therapy, it will be important to have the means to
58 identify the "tissue signature" and "clock window" of ischemic tissues in order to achieve the
59 maximum benefit and to avoid devastating, intraparenchymal hemorrhage (17). Using DWI/
60 PWI to identify potential candidates for i.v. or intra-arterial (i.a.) thrombolysis, especially beyond
61 the currently approved three-hour time window should provide a mechanism to enhance patient
62 selection that could lead to a greater chance for therapeutic benefit. Preliminary open-label stud-
63 ies support this hypothesis as patients treated with thrombolytic therapy beyond three hours,
64 who have a PWI/DWI mismatch, appear to have a reasonably favorable outcome that may even
65 exceed the benefits observed without penumbral imaging, during the three-hour window (19).

66 Similar observations of a PWI/DWI mismatch in animal stroke models have been limited
67 and the temporal evolution of the mismatch on a pixel-by-pixel basis in animal models has yet
68 to be systematically investigated. Animal models in which focal ischemia can be reproducibly
69 studied under controlled conditions are important for identifying and predicting the severity of
70 ischemic injury and for evaluating the efficacy of therapeutic interventions. Characterizing the
71 natural history and predictive value of the PWI/DWI mismatch in animal stroke models is,
72 particularly, important because the PWI/DWI mismatch is being used as an indicator of
73 "ischemic penumbra" in the clinical trial setting. In animal studies, the PWI/DWI mismatch
74 approach could be used to determine the potential therapeutic window for interventions, and
75 to assess the effects of interventions on different components of the ischemic region. It is highly
76 likely that each type of animal stroke model has a different temporal profile for the evolution of
77 the ischemic penumbra and, therefore, the potential for therapeutic intervention. It is even
78 possible that the same model may vary among different laboratories related to subtle differ-
79 ences in technique. Therefore, investigating the PWI/DWI mismatch in different models and
80 locations should prove highly valuable for better characterizing stroke models.

81 The application of DWI and PWI in stroke animal models has a long history and helped to
82 guide their application in human stroke (20). DWI was used to characterize the temporal and
83 spatial evolution of experimental ischemic injury. It was also used as an in vivo assessment tool
84 for both reperfusion and neuroprotective therapy, providing invaluable information about the
85 location and characteristics of ischemic tissue responses to a variety of therapeutic interventions
86 (21). PWI has also been applied to the study of ischemic lesion development and its response to
87 therapy, primarily reperfusion, in several different types of animal stroke models (22). It is
88 particularly useful for evaluating the effect of i.v. or i.a. thrombolysis on the brain's microcircula-
89 tion. These animal DWI and PWI studies have helped to lead the way for the application of these
90 MRI techniques in human stroke studies and trials. Little experimental work has been performed
91 using the PWI/DWI mismatch in animal stroke models to approximate the ischemic penumbra
92 and to characterize the effects of treatment on this tissue.

93 Over the past few years, we and others have developed and applied high-resolution quan-
94 titative perfusion and diffusion imaging protocols in rat stroke models. Figure 1A shows a repre- F1
95 sentative high-resolution quantitative perfusion and diffusion maps obtained at approximately
96 30 minutes postischemic occlusion in Sprague-Dawley rats. The anatomic area defined by ADC
97 reduction is initially smaller than the area of CBF reduction. The perfusion-diffusion mismatch
98 is clearly delineated. The areas defined by ADC reduction expand over time and eventually
99 coincides with the area defined by PWI abnormality, if left untreated. The temporal evolution of
100 the permanent and transient (60 minutes) cerebral ischemia is shown in Figure 1B. The lesion
101 volumes were defined based on ADC and CBF viability thresholds validated previously by our
102 laboratory (23). As would be expected, in the permanent occlusion group, the perfusion-defined
103 lesion volume remained relatively constant over time. The diffusion imaging-defined lesion
104 volume was initially small and grew over time to match the perfusion-defined lesion volume.
105 The ADC- and CBF-defined lesion volumes at 180 minutes after stroke onset were similar to the
106 histologically defined triphenyltetrazolium chloride (TTC) infarct volume at 24 hours.

107 In an experiment using Sprague-Dawley rats, reperfusion at 60 minutes immediately
108 reduced the CBF- and ADC-defined lesion volumes. However, the ADC-defined lesion volume
109 grew slightly over time after reperfusion and the infarct volume at 24 hours was slightly larger
110 than the DWI-defined lesion volume at 180 minutes, probably a result of delayed cell death or
111 secondary injury in reperfused tissue. Both the ADC-defined lesion volume at 180 minutes and
112 TTC infarct volume at 24 hours were significantly smaller than those observed with permanent



138
139
140
141
142
143

FIGURE 1 (A) Representative apparent diffusion coefficient (ADC) and cerebral blood flow (CBF) maps from one animal at 30 minutes postocclusion. The grayscale bar indicates ADC ranges from 0 to 0.001 mm²/sec and CBF ranges from 0 to 2 mL/g/min. (B) Temporal progression of ADC- and CBF-defined lesion volumes of permanent ($n = 6$) and transient (60 minutes, $n = 6$) occlusion determined by using the group-average viability thresholds 57% and 30% reduction for CBF and ADC thresholds, respectively. Histological triphenyltetrazolium chloride infarction volumes are also displayed. *Source:* From Ref. 17.

144
145

occlusion, supporting the concept that early reperfusion will salvage a portion of the ischemic region.

146
147
148
149
150
151
152
153
154
155
156
157

We had also investigated the dynamic evolution of ischemic injury in a different rat strain, Wistar rats, which are known to have better collateral blood flow (24). In the Wistar rats that underwent permanent occlusion, a significant mismatch of PWI to DWI volume was observed up to 90 minutes after middle cerebral artery occlusion (MCAO) (25). At this time point, in the Sprague-Dawley group, the mismatch volume was no longer statistically significant. The experiments were performed under identical conditions so that the only difference was the rat strain employed and appear to demonstrate that the strain of rats used in an experiment can influence the dynamics of penumbral evolution. These studies together demonstrate how DWI and PWI can be used to follow the evolution of ischemic injury, the PWI/DWI mismatch region, and the effects of mechanical reperfusion on in vivo tissue injury and how differences in experimental conditions can be used to follow the evolution of the PWI/DWI mismatch.

158 159 160

AUTOMATED CLUSTER ANALYSIS

161
162
163
164
165
166
167
168

Most of the analysis of stroke data were carried out using a volumetric approach and involved the use of a region-of-interest (ROI) analysis. Although ROI analysis is helpful in simplifying a complex analysis problem, these contain tissues with different ADC and CBF characteristics, thereby inadvertently mixing the characteristics that one is trying to resolve and oversimplifying the complex task of assessing tissue viability. The complex temporal and spatial evolution of focal cerebral ischemia has recently prompted the use of various combinations of MR parameters and more sophisticated analysis methods (26–31) for performing multiparametric segmentation on a pixel-by-pixel basis to predict stroke outcome. These methods could significantly enhance the use of MRI for accurate diagnosis and prognosis of stroke. One of the most well-known

169 multiparametric segmentation approaches is the iterative self-organizing data analysis technique
 170 (ISODATA). Jacobs et al. (27) employed the ISODATA technique to analyze T_2 , T_1 , and DWI
 171 stroke data in both animals (26) and humans, during the subacute phase where T_1 and T_2 were
 172 informative. Wu et al. (30) used generalized linear model algorithms to analyze DWI and PWI
 173 data to predict tissue outcome in human stroke patients scanned within 12 hours of symptom
 174 onset. Essentially, all of the studies, mentioned earlier, focused on the subacute stage when the
 175 DWI-defined ischemic lesions had essentially stopped evolving. Furthermore, qualitative PWI
 176 and DWI were often used due to time constraint and/or technical limitations in the MRI data
 177 acquisition. Cluster analysis of quantitative perfusion and diffusion imaging could potentially
 178 yield a finer discrimination of tissue status based on their intrinsic diffusion and perfusion
 179 characteristics during the acute phase.

180 Our lab recently implemented a modified ISODATA technique with some improved figures
 181 (32). Figure 2 shows the results of the modified ISODATA analysis in a stroke rat. In contrast to F2
 182

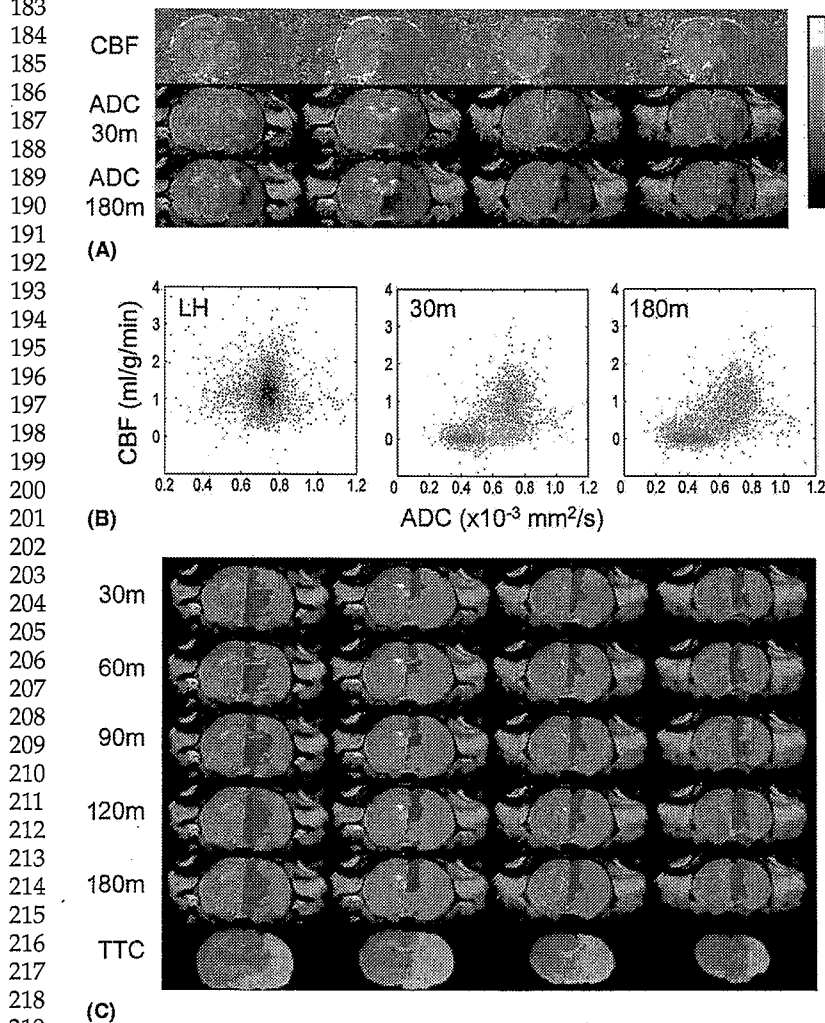


FIGURE 2 Iterative self-organizing data analysis technique (ISODATA) analysis of different ischemic tissue types. (A) cerebral blood flow (CBF) maps, and apparent diffusion coefficient (ADC) maps at 30 minutes and 180 minutes. The greyscale bar: ADC ranges from 0 to 0.001 mm²/sec, CBF ranges from 0 to 2 mL/g/min. (B) CBF-ADC scatterplots of the normal left hemisphere at 30 minutes, ISODATA cluster analysis results of the right hemisphere at 30 and 180 minutes. (C) Pixel clusters from the CBF-ADC scatterplots were overlaid on the image space at 30, 60, 90, 120, and 180 minutes. In the right hemisphere, blue, green, and red are assigned as "normal," "perfusion-diffusion" mismatch, and "ischemic core" clusters, respectively. Triphenyltetrazolium chloride slides at 24 hours are also shown.

225 the normal left hemisphere that exhibited a single cluster, the right ischemic hemisphere showed
 226 three distinct clusters at 30 minutes, namely: the normal (blue), core (red), and mismatch cluster
 227 (green). At 180 minutes, the scatterplots showed that the mismatch had largely disappeared.
 228 Different pixel clusters resolved on the scatterplots were mapped onto the image spaces.
 229 Mismatch was located peripheral to the ischemic core. The ischemic "core" volumes grew and
 230 the "mismatch" volumes decreased as ischemia progressed. The ISODATA-derived lesion vol-
 231 umes showed excellent slice-by-slice correspondence with the TTC infarct volumes. A correla-
 232 tion analysis was performed between the ISODATA-derived lesion volumes and TTC infarct
 233 volumes for each animal, at each time point postocclusion. The correlation coefficients with
 234 respect to the unity line for 30, 60, 90, 120, and 180 minutes postischemia were 0.62, 0.74, 0.83,
 235 0.94, 0.99, respectively. These results demonstrated that the automated cluster analysis yielded
 236 objective classification of different ischemic tissue types.

237 238 PREDICTING ISCHEMIC TISSUE FATES

239 In addition to ischemic tissue characterization, MRI data obtained early after stroke onset also
 240 offers the unique opportunity to statistically predict ischemic tissue fate. Welch et al. (27) used Q_2
 241 a threshold-based analysis and demonstrated that the combination of T_2 and ADC data
 242 provided improved prediction of infarction relative to either parameter alone, in subacute
 243 stroke in humans. Wu et al. (30) reported the eloquent use of a generalized linear model to
 244 predict stroke outcomes based on DWI, PWI, and T_2 data in humans. Lesions were defined
 245 using a threshold-based method to generate the training set. However, this approach appears
 246 less intuitive as the contribution of various parameters is difficult to assess. We developed and
 247 validated a simple and intuitive statistical algorithm for predicting ischemic tissue fate after
 248 acute ischemic stroke in a well-characterized rat stroke (permanent suture occlusion) model
 249 (32). Quantitative high-resolution perfusion and diffusion imaging were obtained. A modified
 250 ISODATA cluster analysis (as opposed to a threshold-based analysis) was used to classify
 251 tissue types. Prediction of tissue infarct was made for overall tissue fate as well as for individ-
 252 ual ISODATA-defined pixel clusters (such as normal tissue, ischemic "penumbra," and
 253 ischemic core) by comparing the in vivo MRI data to TTC-confirmed infarction at 24 hours.
 254 Probability profiles were derived. Prediction using ADC data alone, CBF data alone, and
 255 CBF + ADC data were compared and correlated with endpoint imaging and histology. The
 256 resultant prediction maps were not used to identify tissue infarction but to predict risk of
 257 future infarction. Performance measures of the prediction, such as sensitivity, specificity, and
 258 receiver operating characteristic, were also evaluated.

259 Two-dimensional probability of infarct (P_I) contour plots based on the combined ADC + CBF
 260 data at different time points postischemia were computed (Fig. 3A). Pixels with low ADC and low P_I
 261 CBF showed high P_I . The "mismatch" zone, in which the ADC was normal or near normal but the P_I
 262 CBF was reduced, dynamically evolved and showed a nonzero P_I (>20%). The P_D contour plot
 263 showed two modes at 30 minutes postischemia and a single mode at subsequent time points. As
 264 ischemia progressed, the P_I contour plots became sharper with the highest probability density
 265 remained relatively time invariant ($ADC \sim 0.42 \times 10^{-3} \text{ mm}^2/\text{sec}$ and $CBF \sim 0 \text{ mL/g/min}$).

266 Probability maps of risk of subsequent infarction were computed on a separate group of
 267 animals. Figure 3B shows the probability maps of future infarction based on the 30-minute
 268 ADC, CBF, and ADC + CBF data from one animal. For comparison, ADC and CBF maps at 30
 269 and 180 minutes, ISODATA analysis of the 180-minute data, and 24-hour TTC histology are also
 270 displayed. Prediction made with ADC data alone underestimated infarct volume, whereas pre-
 271 dictions made with CBF data alone overestimated infarct volume. With the combined ADC + CBF
 272 data, most of the mismatch pixels (circular ROI in the inset) were predicted correctly to go into
 273 infarct (i.e., correlated with histology and ISODATA results), whereas with ADC data alone, the
 274 mismatch was incorrectly predicted not to go into infarct. Furthermore, with the combined
 275 ADC + CBF information, most of the "normal" pixels in the right hemisphere (rectangular ROI
 276 in the inset) was predicted to remain normal with significantly higher certainty ($P_I \sim 0$), whereas
 277 with CBF data alone, most of the "normal" pixels were incorrectly predicted to have substantial
 278 nonzero probability of going into infarct. Predicted infarct volumes based on the ADC + CBF
 279 data showed the best correspondence with the ISODATA maps and the 24-hour TTC infarct
 280 volumes.

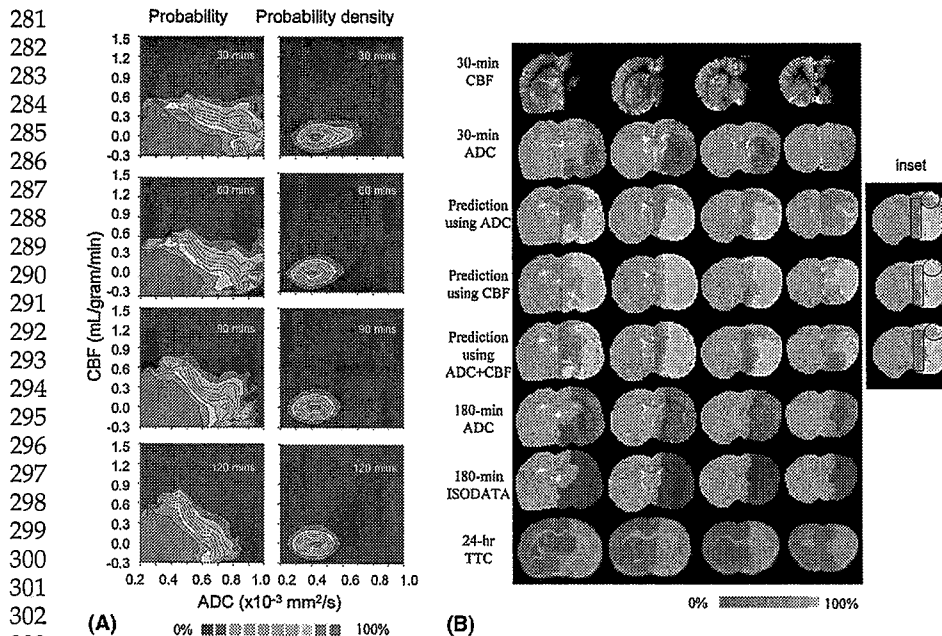


FIGURE 3 Profiles of probability of infarct and probability density of infarct as a function of (A) apparent diffusion coefficient (ADC) + cerebral blood flow (CBF) at different time points postischemia (training Group A, $n=6$). Blue–red color bar indicates the probability ranging from 0% to 100% in steps of 10%. Probability density profiles were normalized from 0% to 100%. Probability maps of risk of future infarction determined based on the 30-minutes ADC data alone, CBF data alone, and ADC+CBF data from a representative animal (experimental Group B). Multislice images are displayed from left to right as posterior to anterior slices. Also shown are the 30-minute ADC and CBF maps, 180-minute ADC maps, iterative self-organizing data analysis technique analysis at 180 minutes, and 24-hour triphenyltetrazolium chloride staining. Hypointensities in the ADC and CBF maps indicate regions of reduced ADC and CBF values, respectively. Red–yellow color bar indicates the probability of infarct ranging from 0% to 100% in steps of 10%. The inset shows prediction using ADC alone underestimated infarct volume whereas CBF alone overestimated infarct volume [circular region-of-interest (ROI)]. Prediction using ADC+CBF showed “normal” tissues having a high degree of certainty of not going into infarct (low probability, rectangular ROI) relative ADC or CBF alone.

Receiver-operating-characteristic (ROC) curves were used to evaluate the accuracy of the predictions made by using ADC alone, CBF alone, and ADC + CBF (Fig. 4A). Predictions made using ADC + CBF data showed slightly higher sensitivity and specificity than those using ADC alone or CBF alone. At the optimal operating points, combined ADC + CBF predicted tissue infarction with $86 \pm 4\%$ sensitivity and $89 \pm 6\%$ specificity.

Although performance measures of overall tissue fate prediction made with ADC+CBF, generally, showed improvement over those made with ADC or CBF alone, the improvement was surprisingly small. This is because the performance measures based on the prediction of overall tissue fate have a poor dynamic range (i.e., good performance is clustered at the very high percentage of sensitivity and specificity) and are dominated by the fate of the “core” pixels. A partial area index was helpful because it samples specific region of under the ROC curve region with a larger dynamic range. However, the choice of the ranges over which the area is integrated is subjective and such ranges could depend on diseases and/or disease stages. The combined automated tissue classification and statistical prediction proposed herein are important because it allowed the performance measures of individual tissue types to be assessed, avoiding the aforementioned drawbacks. Indeed, performance analysis confirmed that the poor dynamic ranges of the ROC curves were dominated by the fate of the already infarcted pixels. Performance measures of individual tissue types should provide a more sensitive and appropriate assessment of the prediction accuracy compared to those of the overall tissue fates. Figure 4B shows the prediction of individual tissue types. Modified ISODATA clustering was used to resolve “normal,” “mismatch,” and “core” pixels and probability of infarct were

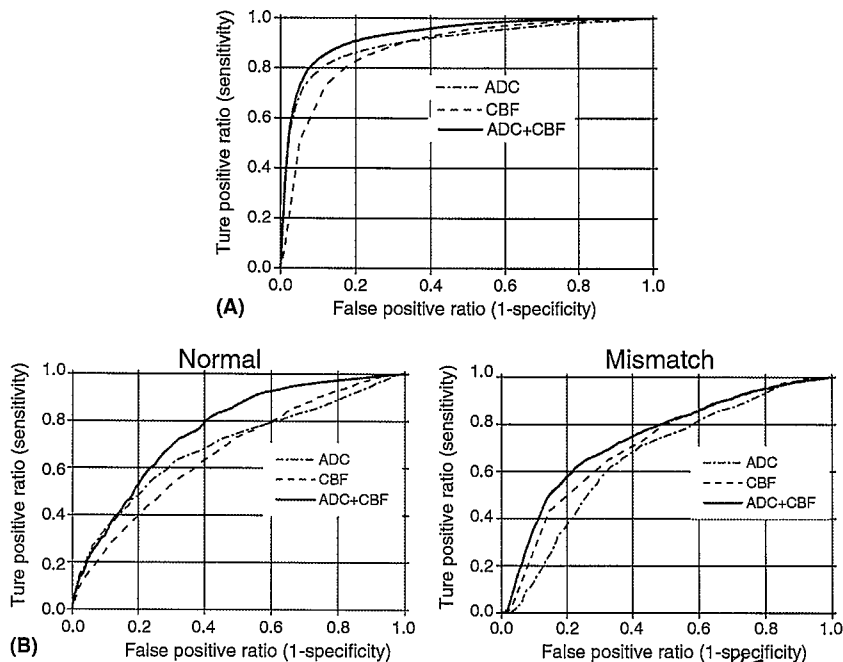


FIGURE 4 Receiver-operating-characteristic curves of sensitivity versus (1-specificity) of the prediction of (A) overall tissue fates and (B) tissue fates of individual iterative self-organizing data analysis technique-derived (normal, mismatch) clusters. Data were derived from incorporating the ADC data, CBF data, and ADC + CBF data (Group B, $n=6$). All standard deviation error bars were <0.05 and are not displayed for clarity.

evaluated for individual tissue types. Prediction of infarct for each tissue type was made and the results were as follows: (i) For the P_I of the right-hemisphere normal cluster, combined ADC + CBF data correctly showed low probability of infarct, whereas ADC data alone and CBF data alone showed substantial probability of infarct. (ii) For the mismatch cluster, combined ADC + CBF data correctly predicted the infarct probability, whereas ADC underestimated the infarct probability and CBF overestimated the infarct probability. The dynamic ranges of sensitivity and specificity of the prediction algorithm made for individual tissue types were larger than those the prediction algorithm made for overall tissue fates. To the best of our knowledge, this is the first statistical prediction of tissue infarction for individual ischemic tissue types.

APPLICATIONS-TO-THERAPY

Based upon our observations for penumbral survival using the PWI/DWI mismatch temporal profile, we predicted that initiation of therapy at 60 minutes after MCAO in the permanent suture occlusion model could yield substantial tissue salvage with neuroprotection. Dimethyl sulfoxide (DMSO) was evaluated and compared to a saline control group (33). A 33% solution of DMSO or saline was initiated at 60 minutes and then infused for three hours for a total dose of 1.5 g/kg of DMSO. Serial DWI and PWI studies were performed and demonstrated a large initial region of PWI abnormality that persisted over time (Fig. 5). The DWI abnormal region initially increased but when the DMSO infusion was started no further growth occurred over the subsequent three hours and the TTC-confirmed infarct volume at 24 hours was reduced by more than 40% in the DMSO group compared to the control group ($P = 0.002$). The absolute ADC values in the PWI/DWI mismatch region were characterized in the DMSO-treated and control groups. The ADC values progressively declined in the mismatch region over time in the control group but declined only slightly in the DMSO group. This study demonstrates that DMSO, initiated 60 minutes after MCAO in this permanent occlusion model, was highly protective and prevented the PWI/DWI mismatch region, probably representing the ischemic

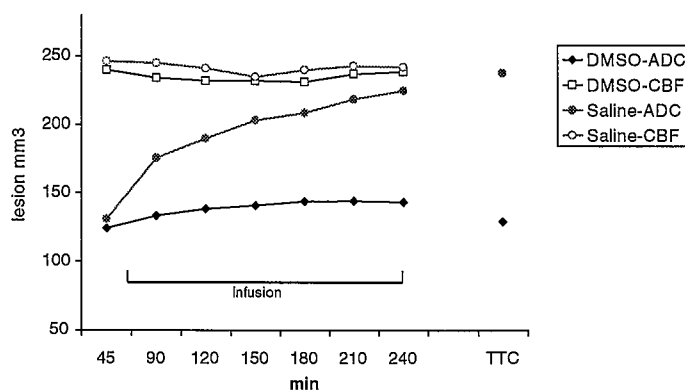


FIGURE 5 The perfusion and diffusion lesion volumes evolve differently over time in DMSO and saline vehicle treated animals with dimethyl sulfoxide treatment essentially preventing further enlargement of the diffusion lesion volume.

penumbra from evolving into infarction. Follow-up benchtop studies with DMSO demonstrated that three-day survival with the same treatment paradigm maintained the protective effect and that initiation of the therapy at two hours after MCAO did not demonstrate a significant effect on infarct volume reduction. Interestingly, the infarct volume observed in the two-hour DMSO treatment group was almost identical to the DWI lesion volume observed at two hours in the control group of the MRI experiment.

In a second preliminary MRI experiment using normobaric hyperoxia as the therapeutic intervention, the initial results appear to be somewhat different. Prior studies with normobaric hyperoxia suggested that this therapy is effective in reducing infarct size in temporary MCAO models but not with permanent occlusion (34). Additionally, normobaric hyperoxia was shown to extend the time window for successful treatment with i.v. t-PA in a rat stroke model (35). We observed that normobaric hyperoxia, when initiated 30 minutes after initiation of permanent MCAO, dramatically reduced the expansion of the DWI-determined lesion volume during the three hours of treatment without any effect on the PWI-lesion volume. However, after stopping treatment, the DWI lesion volume began to grow again within 30 minutes of cessation and the TTC-determined infarct volume at 24 hours was almost the same as untreated animals. This preliminary MRI experiment appears to also show that normobaric hyperoxia is effective in the PWI/DWI mismatch region but the effect is lost when treatment stops—a different pattern than that observed with DMSO.

CONCLUSIONS

High-resolution quantitative perfusion and diffusion imaging offers a useful means to evaluate ischemic brain injury. An automated ISODATA analysis of the ADC and CBF tissue characteristics during the acute phase provides a powerful and unbiased means to characterize tissue fates in ischemic brain injury, and to monitor therapeutic intervention. Combined with the probabilistic prediction algorithm, risk of future infarction could be statistically estimated. These advances are expected to be useful for staging and monitoring the spatiotemporal dynamics of ischemic brain injury on a pixel-by-pixel basis as a function of therapeutic intervention in both animals and, eventually, humans. In treatment experiments, the mismatch-defined penumbra could be persistently salvaged with DMSO and transiently prevented from evolving with normobaric hyperoxia.

REFERENCES

1. Moseley ME, Cohen Y, Mintorovitch J, et al. Early detection of regional cerebral ischemia in cats: comparison of diffusion- and T2-weighted MRI and spectroscopy. *Magn Reson Med* 1990; 14:330–346.
2. Zhong J, Petroff AC, Prichard JW, Gore JC. Changes in water diffusion and relaxation properties of rat cerebrum during status epilepticus. *Magn Reson Med* 1993; 30:241–246.

- 449
450
451
452
453
454
455
456
457
458
459
460
461
462
463
464
465
466
467
468
469
470
471
472
473
474
475
476
477
478
479
480
481
482
483
484
485
486
487
488
489
490
491
492
493
494
495
496
497
498
499
500
501
502
503
504
3. van der Toorn A, Dijkhuizen RM, Tulleken CAF, Nicolay K. Diffusion of metabolites in normal and ischemic rat brain measured by localized ¹H MRS. *Magn Reson Med* 1996; 36:914–922.
 4. Duong TQ, Ackerman JJH, Ying HS, Neil JJ. Evaluation of extra- and intracellular apparent diffusion in normal and globally ischemic rat brain via ¹⁹F NMR. *Magn Reson Med* 1998; 40:1–13.
 5. Busza AL, Allen KL, King MD, van Bruggen N, Williams SR, Gadian DG. Diffusion-weighted imaging studies of cerebral ischemia in gerbils: Potential relevance to energy failure. *Stroke* 1992; 23:1602–1612.
 6. Mancuso A, Karibe H, Rooney WD. Correlation of early reduction in the apparent diffusion coefficient of water with blood flow reduction during middle cerebral artery occlusion in rats. *Magn Reson Med* 1995; 34:368–377.
 7. Calamante F, Thomas DL, Pell GS, Wiersma J, Turner R. Measuring cerebral blood flow using magnetic resonance imaging techniques. *J Cereb Blood Flow Metab* 1999; 19:701–735.
 8. Williams DS, Detre JA, Leigh JS, Koretsky AP. Magnetic resonance imaging of perfusion using spin inversion of arterial water. *Proc Natl Acad Sci U S A* 1992; 89:212–216.
 9. Roussel SA, van Bruggen N, King MD, Housemen J, Williams SR, Gadian DG. Monitoring the initial expansion of focal ischemic changes by diffusion-weighted MRI using a remote controlled method of occlusion. *NMR in Biomed* 1994; 7:21–28.
 10. Warach S, Dashe J, Edelman R. Clinical outcome in ischemic stroke predicted by early diffusion-weighted and perfusion magnetic resonance imaging. *J Cereb Blood Flow Metab* 1996; 16:53–59.
 11. Hoehn-Berlage M, Norris DG, Kohno K, Mies G, Leibfritz D, Hossmann K-A. Evolution of regional changes in apparent diffusion coefficient during focal ischemia of rat brain: The relationship of quantitative diffusion NMR imaging to reduction in cerebral blood flow and metabolic disturbances. *J Cereb Blood Flow Metab* 1995; 15:1002–1011.
 12. Back T, Hoehn-Berlage M, Kohno K, Hossmann K-A. Diffusion nuclear magnetic resonance imaging in experimental stroke correlation with cerebral metabolites. *Stroke* 1994; 25:494–500.
 13. Kohno K, Hoehn-Berlage M, Mies G, Back T, Hossmann KA. Relationship between diffusion-weighted MR images, cerebral blood flow, and energy state in experimental brain infarction. *Magn Reson Imag* 1995; 13:73–80.
 14. Parsons MW, Yang Q, Barber A, et al. Perfusion magnetic resonance imaging maps in hyperacute stroke relative cerebral blood flow most accurately identifies tissue destined to infarct. *Stroke* 2001; 32:1581–1587.
 15. Schlaug G, Benfield A, Baird AE, et al. The ischemic penumbra: operationally defined by diffusion and perfusion MRI. *Neurology* 1999; 53:1528–1537.
 16. Kaufmann AM, Firlik AD, Fukui MB, Weshler LR, Jungries CA, Yonas H. Ischemic core and penumbra in human stroke. *Stroke* 1999; 30:93–99.
 17. Albers GW. Expanding the window for thrombolytic therapy in acute stroke: The potential role of acute MRI for patient selection. *Stroke* 1999; 30:2230–2237.
 18. NINDS. Tissue plasminogen activator for acute ischemic stroke. The National Institute of Neurological Disorder, and Stroke rt-PA Stroke Study Group. *N Engl J Med* 1995; 333:1581–1587.
 19. Ribo M, Molina CA, Rovira A, et al. Safety and efficacy of intravenous tissue plasminogen activator stroke treatment in the 3- to 6- hour window using multimodal transcranial/doppler MRI selection protocol. *Stroke* 2005; 36:602–606.
 20. van Bruggen N, Roberts TP, Cremer JE. The application of magnetic resonance imaging to the study of experimental cerebral ischemia. *Cerebrovasc Brain Metab Rev* 1994; 6:180–210.
 21. Li F, Carano RAD, Irie K, et al. Neuroprotective effects of a novel broad spectrum cation channel blocker LOE 908M5 on experimental focal ischemia. *JMRI* 1999; 10:138–145.
 22. Takano K, Carano RAD, Tatlisumak T, et al. The efficacy of intraarterial and intravenous Prourokinase in an embolic stroke model evaluated by diffusion-perfusion magnetic resonance imaging. *Neurology* 1998; 50:870–875.
 23. Shen Q, Meng X, Fisher M, Sotak CH, Duong TQ. Pixel-by-pixel spatiotemporal progression of focal ischemia derived using quantitative perfusion and diffusion imaging. *J Cereb Blood Flow Metab* 2003; 23:1479–1488.
 24. Oliff HS, Coyle P, Weber E. Rat strain and vendor differences in collateral anastomoses. *J Cereb Blood Flow Metab* 1997; 17:571–578.
 25. Bardutzky J, Shen Q, Ren H, et al. Differences in ischemic lesion evolution in different rat strains using diffusion and perfusion imaging. *Stroke* 2005; 36:2000–2005.
 26. Welch KM, Windham J, Knight RA, et al. A model to predict the histopathology of human stroke using diffusion and T2-weighted magnetic resonance imaging. *Stroke* 1995; 26:1983–1989.
 27. Jacobs MA, Mitsias P, Soltaniaan-Zadeh H, et al. Multiparametric MRI tissue characterization in clinical stroke with correlation to clinical outcome: part 2. *Stroke* 2001; 32:950–957.
 28. Mitsias PD, Jacobs MA, Hammond R, et al. Multiparametric MRI ISODATA ischemic lesion analysis correlation with the clinical neurological deficit and single-parameter MRI techniques. *Stroke* 2002; 33:2839–2844.
 29. Carano RA, Li F, Irie K, et al. Multispectral analysis of the temporal evolution of cerebral ischemia in the rat brain. *J Magn Reson Imag* 2000; 12:842–858.

- 505 30. Wu O, Koroshetz WJ, Ostergard L, et al. Predicting tissue outcome in acute human cerebral ischemia
506 using combined diffusion-and perfusion-weighted MR imaging. *Stroke* 2001; 32:933-942.
- 507 31. Jacobs MA, Zhang ZG, Knight RA, et al. A model for multiparametric mri tissue characterization in
508 experimental cerebral ischemia with histological validation in rat: part 1. *Stroke* 2001; 32:943-949.
- 509 32. Shen Q, Ren H, Bouley J, Fisher M, Duong TQ. Dynamic tracking of acute ischemic tissue fates using
510 improved unsupervised ISODATA analysis of high-resolution quantitative perfusion and diffusion
511 data. *J Cereb Blood Flow Metab* 2004; 24:887-897.
- 512 33. Bardutsky J, Meng X, Bouley J, Duong TQ, Ratan R, Fisher M. Effects of IV dimethyl sulfoxide on
513 ischemia evolution in permanently occluded rats. *J Cereb Blood Flow Metab* 2005; 25:968-977.
- 514 34. Singhal AB, Dijkhuizen RM, Rosen BR, Lo EH. Normobaric hyperoxia reduces MRI diffusion
515 abnormalities and infarct size in experimental stroke. *Neurology* 2002; 58:945-952.
- 516 35. Kim HY, Singhal AB, Lo EH. Normobaric hyperoxia extends the reperfusion window in focal cerebral
517 ischemia. *Ann Neurol* 2005; 57:571-575.
- 518
- 519
- 520
- 521
- 522
- 523
- 524
- 525
- 526
- 527
- 528
- 529
- 530
- 531
- 532
- 533
- 534
- 535
- 536
- 537
- 538
- 539
- 540
- 541
- 542
- 543
- 544
- 545
- 546
- 547
- 548
- 549
- 550
- 551
- 552
- 553
- 554
- 555
- 556
- 557
- 558
- 559
- 560